Pyrolysis Kinetics of a Green River Oil Shale Using a Pressurized TGA

ARTICLE *in* ENERGY & FUELS · DECEMBER 2010

Impact Factor: 2.79 · DOI: 10.1021/ef101115u

Energy Fuels **2011,** *25,* 232–239 · DOI:10.1021/ef101115u
Published on Web 12/20/2010

energy&fuels
article

Pyrolysis Kinetics of a Green River Oil Shale Using a Pressurized TGA

James L. Hillier and Thomas H. Fletcher*

Chemical Engineering Department, 350 CB, Brigham Young University, Provo, Utah 84602, United States

Received August 19, 2010. Revised Manuscript Received December 3, 2010

Crushed samples of Green River Oil Shale and its kerogen extract were pyrolyzed at heating rates from 1 to 10 K/min at pressures of 1 and 40 bar and temperatures up to 1000 °C. Two to four mass release peaks were observed with the major two corresponding to kerogen pyrolysis and carbonate decomposition. The transient pyrolysis data were fit with a first-order model and a Distributed Activation Energy Model (DAEM). An F-test was used to determine confidence regions and compare the kinetic parameters among the oil shale and demineralized samples, between the two pressure levels, and between the models. The activation energies determined ranged from 173 to 226 kJ/mol, while the pre-exponential factors ranged from 2.74×10^{10} to 1.86×10^{14} 1/s. It was found that there is not a significant difference among the activation energy/pre-exponential factor combinations determined for oil shale and the demineralized samples nor between pressures of 1 and 40 bar. The first-order and DAEM models were also shown to be statistically different, but both models performed well.

Introduction

Thermogravimetric analysis (TGA) is a common technique to determine global kinetic parameters for complex reactions.[1−6] Global kinetic parameters obtained from TGA can be used to describe reaction behavior over a wide range of heating rates and temperatures.[7] Isothermal TGA experiments have utilized by many researchers[6,8−10] for slow reactions. Rate constants (k) measured from multiple isothermal experiments at various temperatures lead to determination of activation energy (E) and frequency factor (A) using a $\ln k$ vs $1/T$ plot. Nonisothermal experiments are carried out by heating the sample at a given rate and measuring the residual mass with respect to time. The data are then regressed by fitting an equation to the linearized form of the data or some other regression technique. Nonisothermal techniques are often used in pyrolysis experiments because the reactions occur during sample heatup before an isothermal state can be achieved.

A partial list of researchers employing TGA methods (and a few other pyrolysis methods) for oil shale pyrolysis is shown in Table 1 along with the reported kinetic parameters. Some of these parameters are quite different even despite coming from different formations. It is noted that some investigators have reported different activation energies for each heating rate. Brown et al. note that multiple heating rates are most effective in determining kinetic parameters[11] (as opposed to different parameters for each heating rate) and Maciejewski notes that the use of a single heating rate is to be avoided.[12] The practice of having a different set of kinetic parameters for each heating rate is most likely erroneous for experiments conducted in both the kinetically limiting range (where one set of parameters should be able to describe the different heating rates) and the mass transfer limited range.

In Table 1 the samples come from many formations around the world including the Green River formation in the United States. The Green River deposit is one of the largest formations of oil shale with an estimated 1.8 trillion barrels of oil equivalent[13] and has been the subject of many pyrolysis studies.

Part of this study is to observe the kinetic effect (if any) of the interaction between kerogen and oil shale (kerogen + minerals) during pyrolysis for this specific sample. The null hypothesis is that there is no difference. To observe whether this holds true for Sample A and its derivatives, the organic portion can be separated from the mineral matrix by a series of acid washes.[29,30] A slightly modified version of the extraction used by Winans and co-workers[29] was used in this study. Pyrolysis of demineralized kerogen can then be compared

*To whom correspondence should be addressed. E-mail: tom_fletcher@byu.edu.

(1) Granoff, B.; Nuttall, H. E. Pyrolysis kinetics for oil-shale particles. *Fuel* **1977**, *56* (3), 234–240.
(2) Shuyuan, L.; Zhe, Y.; Jialin, Q.; Shaohui, G. Thermogravimetric kinetics study on some Chinese oil shales. *Oil Shale* **2001**, *18* (4), 307–314.
(3) Abu-Qudais, M.; O. J., J.; Sawalha, S. Kinetics of pyrolysis of Attarat oil shale by thermogravimetry. *Oil Shale* **2005**, *22* (1), 51–63.
(4) Skala, D.; Kopsch, H.; Sokic, M.; Neumann, H. J.; Jovanovic, J. A. Kinetics and modelling of oil shale pyrolysis. *Fuel* **1990**, *69* (4), 490–496.
(5) Williams, P. T.; Ahmad, N. Influence of process conditions on the pyrolysis of Pakistani oil shales. *Fuel* **1999**, *78* (6), 653–662.
(6) Campbell, J. H.; Koskinas, G. H.; Stout, N. D. Kinetics of oil generation from Colorado oil shale. *Fuel* **1978**, *57* (6), 372–376.
(7) Freund, H.; Kelemen, S. R.; Walters, C. C.; Siskin, M.; Gorbaty, M. L.; Curry, D. J.; Bence, A. E. Predicting oil and gas compositional yields via chemical structure-chemical yield modeling (CS-CYM): Part 1 - Concepts and implementation. *Org. Geochem.* **2007**, *38* (2), 288–305.
(8) Lee, S., *Oil Shale Technology*; CRC Press: Boca Raton, FL, 1991; p 261.
(9) Doyle, C. D. Kinetic analysis of thermogravimetric data. *J. Appl. Polym. Sci.* **1961**, *5* (15), 285–292.
(10) Williams, P. T.; Ahmad, N. Investigation of oil-shale pyrolysis processing conditions using thermogravimetric analysis. *Appl. Energy* **2000**, *66* (2), 113–133.
(11) Brown, M. E.; Maciejewski, M.; Vyazovkin, S.; Nomen, R.; Sempere, J.; Burnham, A.; Opfermann, J.; Strey, R.; Anderson, H. L.; Kemmler, A.; Keuleers, R.; Janssens, J.; Desseyn, H. O.; Li, C.-R.; Tang, T. B.; Roduit, B.; Malek, J.; Mitsuhashi, T. Computational aspects of kinetic analysis.: Part A: The ICTAC kinetics project-data, methods and results. *Thermochim. Acta* **2000**, *355* (1−2), 125–143.
(12) Maciejewski, M. Computational aspects of kinetic analysis.: Part B: The ICTAC Kinetics Project -- the decomposition kinetics of calcium carbonate revisited, or some tips on survival in the kinetic minefield. *Thermochim. Acta* **2000**, *355* (1−2), 145–154.
(13) Andrews, A. *Oil Shale: History, Incentives, and Policy*; CRS Report for Congress: April 13, 2006, 2006.
(14) Abu-Qudais, M.; Jaber, J. O.; Sawalha, S. Kinetics of Pyrolysis of Attarat Oil Shale by Thermogravimetry. *Oil Shale* **2005**, *22* (1), 51–63.

Table 1. Researchers Employing Non-Isothermal TGA (And a Few Other) Techniques to Determine the Kinetics of Oil Shale Pyrolysis and Oil Generation (Notice the Spread in the Reported Values. "~" Means Not a Distributed Model)

author(s)	sample	experimental setup	heating rate(s) (K/min)	A (s^{-1})	E (or Eavg) (kJ/mol)	σ (kJ/mol)
Abu-Qudais et al.[14]	Attarat (Jordian) Oil Shale	TGA	3, 5, 10, 20, 40		79.2−91.7	~
Ahmad and Williams[15]	Kark and Salt Range (Pakistan) Oil Shale	TGA	20		68−110, 58−93	~
Avid et al.[16]	Khoot (Mongolian) Oil Shale	TGA	92		96.28	~
Benbouzid and Hafsi[17]	bitumen	TGA	5, 10, 20	1.00×10^{3}	37−97	~
Braun[18]	GROS	Pyrolysis TQ-MS	1, 10	5×10^{13}	221	not available
Burnham[19]	GROS	Pyromat II	0.033, 2	1.1×10^{15}	241	5.8
Campbell et al.[20]	Green River (USA) Oil Shale	TGA	2		149	~
Dogan and Uysal[21]	Turkish Oil Shale	TGA	20		12.5−43.4	~
Jaber and Probert[22]	Ellujun and Sultani (Jordan)	TGA	20, 30, 40, 50	-1.00×10^{-5} to -1.93×10^{-3}	39−68	~
Kök and Pamir[23]	Can, Mengen, and Himmetoglu (Turkish) Oil Shales	TGA	10		24−57	~
Kök and Iscan[24]	Can, Mengen, and Himmetoglu (Turkish) Oil Shales	TGA	5		13.1−215.4	~
Li and Yue[25]	Chinese Oil Shale and GROS	TGA	5		160−200 (dominant rxns)	~
Linder et al.[26]	Swedish Oil Shale	TGA	3.5−21.3		130	~
Rajeshwar[27]	GROS	TGA	5, 10, 20	9.80×10^{10}	116−209	~
Shih and Sohn[28]	GROS	TGA	1−5	5.63×10^{11}	197	~

with pyrolysis of oil shale to identify possible differences that may indicate mineral interactions. It has been reported that the reaction is catalyzed by the carbonates and inhibited by the silicates.[30] Karabakan and Yurum[30] also report a change in activation energy relative to the amount of demineralization. However, Ballice[31] reported that the removal of pyrites with HNO_3 did not affect the reactivity of the organic material in pyrolysis, though he also stated that the removal of the material soluble in HF increased the conversion in pyrolysis reactions. Furthurmore, Reynolds and Burnham[32] compared the kinetic parameters for some specific shales and determined those for oil shale and its kerogen extract and concluded that, "isolation has little effect on parameters when determining overall pyrolysis kinetics". Winans and co-workers[29] demonstrated that the organic portions could be extracted from the oil shale using a combination of benzene and acid washes. Mraz[33] showed that acid dissolution of the mineral matrix is enhanced by ultrasonic waves. Espitalie and co-workers[34] showed that some catalytic activity is demonstrated by calcium ions, but also stated that the effect may be enhanced because of the system they used to observe the reactivity.

(15) Ahmad, N.; Williams, P. T. Influence of particle grain size on the yield and composition of products from the pyrolysis of oil shales. *J. Anal. Appl. Pyrolysis* **1998**, *46* (1), 31–49.

(16) Avid, B.; Purevsuren, B.; Dugarjav, J. Pyrolysis and thermogravimetric investigation of the Mongolian Khoot oil shale. *Oil Shale* **2000**, *17* (3), 241–251.

(17) Benbouzid, M.; Hafsi, S. Thermal and kinetic analyses of pure and oxidized bitumens. *Fuel* **2008**, *87* (8−9), 1585–1590.

(18) Braun, R. L.; Burnham, A. K.; Reynolds, J. G. Oil and gas evolution kinetics for oil shale and petroleum source rocks determined from pyrolysis-TQMS data at two heating rates. *Energy Fuels* **1992**, *6* (4), 468–474.

(19) Burnham, A. K. Oil evolution from a self-purging reactor: kinetics and composition at 2.degree.C/min and 2.degree.C/h. *Energy Fuels* **1991**, *5* (1), 205–214.

(20) Campbell, J. H.; Koskinas, G. J.; Gallegos, G.; Gregg, M. Gas evolution during oil shale pyrolysis. 1. Nonisothermal rate measurements. *Fuel* **1980**, *59* (10), 718–726.

(21) Dogan, O. M.; Uysal, B. Z. Non-isothermal pyrolysis kinetics of three Turkish oil shales. *Fuel* **1996**, *75* (12), 1424–1428.

(22) Jaber, J. O.; Probert, S. D. Non-isothermal thermogravimetry and decomposition kinetics of two Jordanian oil shales under different processing conditions. *Fuel Process. Technol.* **2000**, *63* (1), 57–70.

(23) Kok, M. V.; Pamir, R. Pyrolysis Kinetics of Oil Shales Determined by DSC and TG/DTG. *Oil Shale* **2003**, *20* (1), 57–68.

(24) Kök, M.; Iscan, A. Oil shale kinetics by differential methods. *J. Therm. Anal. Calorim.* **2007**, *88* (3), 657–661.

(25) Li, S.; Yue, C. Study of pyrolysis kinetics of oil shale. *Fuel* **2003**, *82* (3), 337–342.

(26) Linder, G.; Andersson, L. A.; Bjerle, I. Influence of heating rate on the pyrolysis of oil shale. *Fuel Process. Technol.* **1983**, *8* (1), 19–31.

(27) Rajeshwar, K. The kinetics of the thermal decomposition of green river oil shale kerogen by non-isothermal thermogravimetry. *Thermochim. Acta* **1981**, *45* (3), 253–263.

(28) Shih, S. M.; Sohn, H. Y. Nonisothermal Determination of the Intrinsic Kinetics of Oil Generation from Oil Shale. *Ind. Eng. Chem. Proc. Des. Dev.* **1980**, *19* (3), 420–426.

(29) Vandegrift, G. F.; Winans, R. E.; Scott, R. G.; Horwitz, E. P. Quantitative study of the carboxylic acids in Green River oil shale bitumen. *Fuel* **1980**, *59* (9), 627–633.

(30) Karabakan, A.; Yurum, Y. Effect of the mineral matrix in the reactions of oil shales: 1. Pyrolysis reactions of Turkish Goynuk and US Green River oil shales. *Fuel* **1998**, *77* (12), 1303–1309.

(31) Ballice, L. Effect of demineralization on yield and composition of the volatile products evolved from temperature-programmed pyrolysis of Beypazari (Turkey) Oil Shale. *Fuel Process. Technol.* **2005**, *86* (6), 673–690.

(32) Reynolds, J. G.; Burnham, A. K. Comparison of kinetic analysis of source rocks and kerogen concentrates. *Org. Geochem.* **1995**, *23* (1), 11–19.

(33) Mraz, T.; Rosenvold, R.; DuBow, J.; Rajeshwar, K. Acid dissolution of mineral matrix in Green River oil shale. 2. Effect of ultrasonic field. *Fuel* **1984**, *63* (7), 927–930.

(34) Espitalié, J.; Senga Makadi, K.; Trichet, J. Role of the mineral matrix during kerogen pyrolysis. *Org. Geochem.* **1984**, *6*, 365–382.

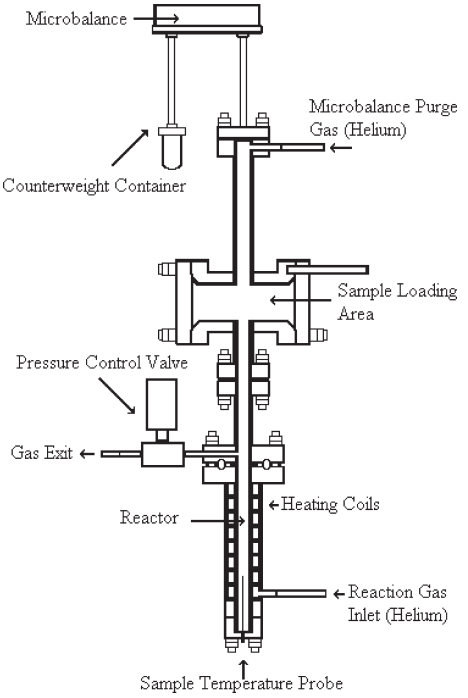

Figure 1. Schematic of the TGA (used with permission from Clayton[35]).

Experimental Section

The oil shale pyrolysis data were acquired using a Deutsche Montan Technologie (DMT) high-pressure thermogravimetric analyzer (HPTGA) rated to a maximum pressure of 100 bar and maximum reactor temperature of 1100 °C. The original data acquisition and control system was replaced. This instrument, prior to the replacement of the control system, was characterized and described previously.[35] A schematic of the apparatus is shown in Figure 1.

Experiments were conducted with approximately 10 mg of sample in a solid (instead of a mesh) Inconel basket weighing approximately 400 mg and measuring 0.9 cm diameter and 0.4 cm tall. The basket was suspended from a thin chain attached to a Sartorius 4404MP8 microbalance. The reactor was purged with He prior to each experiment. Helium was selected because of its high thermal conductivity and low density. This helped to ensure that heat transfer and buoyancy effects were minimized. The TGA was heated via electric heating elements in the reactor vessel. A temperature probe measured the gas temperature near the sample. A temperature calibration wass applied based on the difference between the measured temperature and the known curie point transition temperature of Alumel, nickel, Perkalloy, iron, Hisat50. These metals have curie point transition temperatures that span from 154.2 to 1050 °C, with nickel and Perkalloy (355.3 and 596 °C, respectively) located in the temperature range of interest. Use of standards (acquired from PerkinElmer) provided a multipoint temperature calibration to which a cubic spline was fit, and the temperatures were adjusted on each data set accordingly. Temperature calibrations were performed at each heating rate and pressure combination with replicates to demonstrate the reproducibility of the calibrations for the experimental conditions.

The data for these tests were collected at reactor pressures of 1 and 40 bar (±1%). For the 1 bar tests, gas flow rates of 1.0 L/min through the microbalance and 1.4 L/min through the reactor were used. The 40 bar test used gas flow rates of 2.0 L/min through the microbalance and 3.8 L/min through the reactor. The tests were set to run from 20 to 850 °C (or 950 °C for some high pressure conditions) at 1, 4, and 10 °C/min. Mass data were obtained approximately every second, yielding between 10,000 and 100,000 points.

In the experimental procedure, an assumption was made that the observed reaction rate is a good approximation of the intrinsic reaction rate due to the low heating rates. This means that reaction rate was not significantly hindered by mass transfer effects, and therefore any observed reaction happened in the instant it was observed. To ensure that this assumption was valid a few different actions were taken. Approximately 10 mg of sample was used in each test. With a basket diameter of 9 mm, this gave a large surface area to volume ratio making it easier for the heat and mass to transfer through the entire sample quickly. Second, slower heating rates were used allowing more time for the sample to equilibrate. As the sample is heated at different rates the temperature of highest mass loss rate will shift, which is described using a first-order kinetic model. The difficulty arises when heat and mass transfer effects change the measured and the true sample temperature. Therefore to ensure that the heat transfer effects were negligible three different heating rates were used: 1, 4, and 10 °C/min. A similar test was conducted at 60 °C/min, which showed that the overall shape of the curve differed from the lower heating rates, presumably indicating a heating rate region where heat and mass transfer effects were significant. This agrees with the findings of Torrente et al.[36] that heat transfer effects become a problem for heating rates in excess of 10 °C/min.

The samples used in this experiment are from the Green River formation. Two demineralized samples were used: (1) a sample with the carbonates extracted, and (2) a sample after the final stage of demineralization. In addition, a set of oil shale samples obtained near a surface mine operation were ground and sieved to different particle sizes to verify that the size of the particles did not significantly affect the result. All samples referred to by numbers 1, 2, and 3 are oil shale samples ground to different sizes. These size-graded samples are as follows: (1) samples that are stopped by a 100-mesh sieve (< 149 μm); (2) those which pass through the 100-mesh sieve but are stopped by a 200-mesh sieve (74−149 μm); and (3) those which pass through a 200-mesh sieve but are stopped by a 400-mesh sieve (37−74 μm). Samples A, B, and C refer to the different stages of demineralized oil shale. Sample A is an oil shale with approximately 24% organic mass on a dry basis and was obtained from a core sample. Sample B is a carbonate-free derivative of Sample A. Sample C is a fully extracted kerogen derivative of sample A. Sample A minerals are shown in Table 2 by weight percent as determined by XRD.

The experimental matrix is shown in Table 3 with each experiment being performed at least twice.

Data Reduction

Each set of data was reduced to approximately 1000 data points by boxcar averaging the appropriate number of points and assuming that the irregularities are the result of random noise. The averaged data and the original data were compared to ensure that no important features of the data were lost. Each TGA trace showed between 1 and 4 distinct reaction regions. The number of regions was consistent with the sample. For example, the demineralization stages eliminated regions of carbonate pyrolysis and other reactions at successive stages of the demineralization. The size-graded samples each showed the same number of reaction regions. Each reaction was assumed to be a first-order global reaction with an Arrhenius form of the rate constant. The activation energies were either assumed constant or as a progressive distributed activation energy

(35) Clayton, D. Modeling Flow Effects During Polymer Decomposition Using Percolation Lattice Statistics. Dissertation, Department of Chemical Engineering, Brigham Young University, Provo, UT, 2002.

(36) Torrente, M. C.; Galan, M. A. Kinetics of the thermal decomposition of oil shale from Puertollano (Spain). *Fuel* **2001**, *80* (3), 327–334.

Table 2. Minerals for Sample A as Determined by XRD Rounded to the Nearest Whole Percent (Except Siderite Which Was Rounded up to the Nearest Half Percent)

minerals	percent weight
ank. or exc-Ca dol.	30
K-feldspar	15
calcite	14
quartz	11
organics	9
buddingtonite	6
analcime	6
plagioclase	4
pyrite	1
siderite	0.5
sum non-clay	96
Di 2:1 clay	4
sum clay	4

Table 3. Experimental Matrix

	1 K/min	4 K/min	10 K/min
1 bar	1,2,3,A,B,C	1,2,3,A,B,C	1,2,3,A,B,C
40 bar	1,2,3,A,B,C	1,2,3,A,B,C	1,2,3,A,B,C

similar to that used in the CPD model by Fletcher and coworkers.[37]

Buoyancy effects were a significant factor at elevated temperatures in the TGA. Buoyancy effects coupled with other instrument effects give a nonlinear response function of both temperature and pressure. Clayton[35] generated an apparent mass loss curve by running an empty basket with an inert material to represent the volume of the sample and recording the instrument response. This approach lumped all buoyancy and other effects into an instrument response curve. This is attractive because it includes any specific instrument effects. An example of such a buoyancy curve can be seen in Figure 2. Mohlen and Sulimma[38] employed another buoyancy correction method by calculating buoyancy effects from knowledge of the flow rates and temperature.

The buoyancy correction technique used here is a modification of the Clayton method.[35] Clayton's method was tried first, but there was some variation found in replicates of the blanks. This variation was thought to arise from the orientation of the basket with respect to the flow. Even slight variations could affect the apparent buoyancy. The modification used a blank experiment to determine the form of a correction polynomial, but instead of using a global set of polynomial coefficients for each correction the coefficients were estimated from the initial portion of each individual mass trace. This estimate was performed by first running an empty basket to determine the order of the polynomial (e.g., first or second order). The same order of the polynomial determined for the blank was estimated for each experiment by then fitting the first nonreacting portion of the mass trace to the determined polynomial and correcting the mass based on those parameters. The unreacting portion was determined by heating from temperatures of 20 °C to approximately 200 °C and then back to room temperature. Because sample mass loss was noted to be zero for the samples at these temperatures, a baseline could be established. The buoyancy was then predicted to follow the same

(37) Fletcher, T. H.; Grant, D. M.; Pugmire, R. J.; Kerstein, A. R. Chemical model of coal devolatilization using percolation lattice statistics. *Energy Fuels* **1989**, *3* (2), 175–186.

(38) Mohlen, H. J.; Sulimma, A. High temperature, high pressure thermogravimetry of coal gasification-apparatus, data acuisition and numerical evaluation. *Thermochim. Acta* **1986**, *103* (1), 163–168.

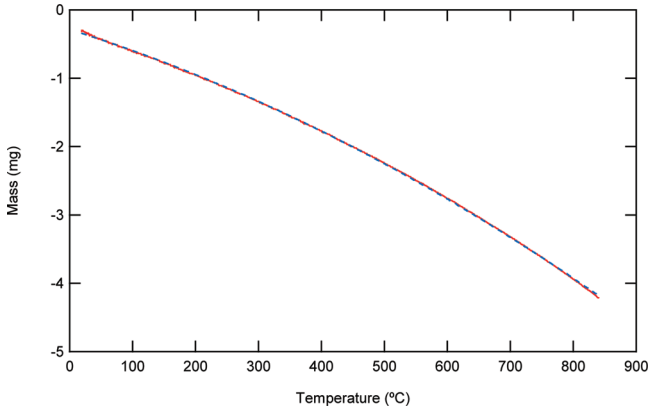

Figure 2. Example instrument response curve in He at 1 bar (solid line) overlaid with a second-order curve fit (dashed line). For this case, $m = aT^2 + bT + c$, and the R^2 value was 0.9999.

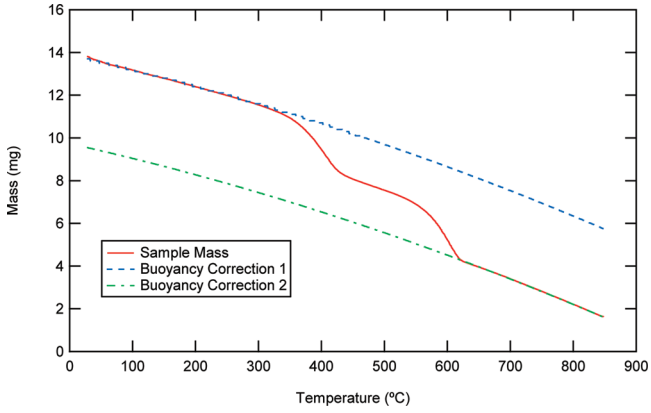

Figure 3. Example buoyancy curves prediction from raw data. Both polynomial curves have the same coefficients but are shifted vertically by a constant value.

polynomial fit throughout the experiment. The justification for this method is shown in Figure 3. Note how the blank basket follows the same curve throughout the entire experiment. The TGA used in this experiment produced a near perfect quadratic curve for a He atmosphere at 1 bar as seen in Figure 2.

Figure 3 shows how the quadratic fits are used to correct for buoyancy throughout a pyrolysis experiment. First the buoyancy curve is predicted from the first 200 °C and then extrapolated over the entire temperature range. A second curve with the same polynomial parameters except a vertical shift is also shown to demonstrate the fit after the reaction has finished. In some cases the temperature region after reactions had finished was also used in refining the buoyancy curve polynomial parameters. The response for the 40 bar condition was closer to linear although the noise was much larger at pressure.

The buoyancy curves were subtracted from the real sample data and then normalized to achieve the final mass curves, as follows.

$$m'_{\text{normal}} = \frac{(m' - m'_{\text{f}})}{(m'_0 - m'_{\text{f}})} \quad (1)$$

where m' is the buoyancy-corrected mass, m'_{f} is the final mass when reaction has stopped (corrected for buoyancy), and m'_0 is the initial mass (corrected for buoyancy). The result of eq 1 is to normalize the mass and to make it range from zero to one.

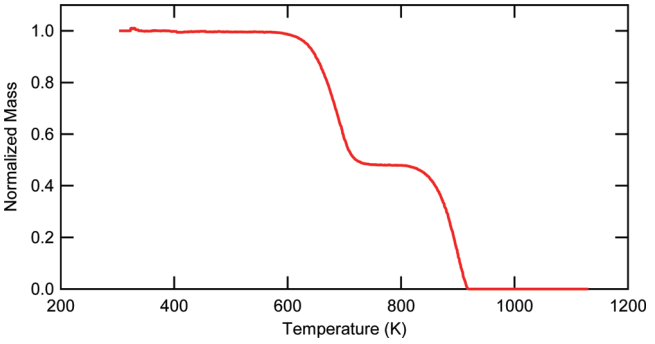

Figure 4. Resulting corrected and normalized mass loss curve from predicted buoyancy shown in Figure 3.

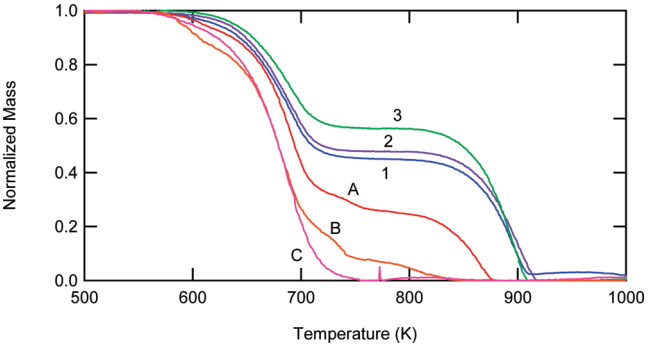

Figure 5. Examples of buoyancy-corrected mass data (1 bar, 1 K/min).

In this way it is related to conversion as the normalized mass equals one minus the conversion. Each sample was reweighed on a separate microbalance after reaction, and the final weight was recorded as a consistency check.

After the resulting corrections are applied the mass shown in Figure 3 becomes the mass shown in Figure 4.

Once the mass traces were corrected and normalized, the kinetic parameters were determined with a method of Hillier and co-workers.[39] The method uses a nonlinear optimization program to match model predictions with measured data. Mass was calculated numerically by integrating differential rate expressions. The method also required that the predicted derivative matched the derivative of the data. The kinetic parameters were determined by an optimized best fit of both the mass curves from three heating rates simultaneously, along with the derivative curves of the mass curves.

Modeling Approach

The pyrolysis data were modeled using (i) a first-order model, shown in eq 2, and (ii) a progressive Distributed Activation Energy Model (DAEM), shown in eq 3.

$$\frac{dm}{dt} = -A \cdot e^{-E/R \cdot T} \cdot m \tag{2}$$

$$\frac{dm}{dt} = -A \cdot e^{-(E \pm \sigma)/R \cdot T} \cdot m \tag{3}$$

The DAEM was applied in a manner similar to that of Fletcher and co-workers.[37] The effective activation energy E is varied about a mean using a Gaussian distribution, defined by E_0 and σ. This distribution is determined as a function of the extent of conversion of the sample. This assumes that material with low activation energy is released first, and that high activation energy material is released last, which seems physically reasonable.

Note that when σ is zero the DAEM becomes the first-order model. This feature lends itself to a comparison between the models using an F-test according to eq 4. In eq 4 SS(θ) represents the error between the model and the data for the set of parameters represented by θ for the respective equation. The subscript 1 represents the first-order model and the 2 represents the DAEM, p is the number of estimated parameters in each model, and n is the number of observations. The null hypotheses, H_0, is that no difference exists between the fits of the two models subject to the comparison of F in eq 4 with critical values as determined from an F distribution.

$$F = \frac{(\mathrm{SS}(\hat{\theta})_1 - \mathrm{SS}(\hat{\theta})_2)/(p_1 - p_2)}{\mathrm{SS}(\hat{\theta})_2/(n - p_2)} \tag{4}$$

Results and Discussion

The objective of this work was to determine global kinetic parameters for specific samples of oil shale and their derivatives from the Green River formation. Typical mass curves are shown in Figure 5. Two peaks were observed in the derivative of the mass curve with temperature for samples 1, 2, and 3 whereas four peaks were observed on sample A. The subsequent stages of demineralization showed three peaks for B and one peak for C. The reaction of interest is the pyrolysis of the organic matter in the shale and occurs between about 600 and 800 K. The reaction that spans this temperature range involves the organic matter whereas the higher temperature reactions involve primarily the mineral matrix. The higher temperature reaction parameters are not included in this analysis.

The parameters in Table 4 were regressed using the method explained briefly above and explained in detail elsewhere.[39] Parameters were regressed for both first-order reaction and distributed activation energy models and Figure 6 shows fits of the two models to the data shown in Figure 5.

As can be seen from Figure 6 both models describe the reaction that occurs between about 620 and 800 K adequately. However, in most of the cases for the organic reaction the DAEM model was statistically better according to the F test and eq 4. Despite this conclusion the magnitude of the distribution parameter (σ) shown in Table 4 was small. This would suggest that a first-order model is indeed sufficient. Figures 7−10 are plots of the parameters in Table 4; confidence regions are determined around each parameter by eq 5.

$$\mathrm{SS}(\theta) \leq \mathrm{SS}(\hat{\theta}) \cdot \left(1 + \frac{p}{n-p} \cdot F_{p,n-p,1-\alpha}\right) \tag{5}$$

In eq 5, θ represents the vector of parameters regressed from either eq 2 or 3, $\hat{\theta}$ represents the optimal parameters, and F is the inverse distribution as a function of the confidence level, α, and the degrees of freedom. As in eq 4, n is the number of observations and p is the number of parameters. From observation of eq 5 there are two methods of shrinking the size of the critical value (i.e., the RHS of eq 5) used in constructing the confidence regions for a given model at a given confidence level. The first is to increase the number of observations. This affects the portion of the RHS of eq 5 enclosed in the

(39) Hillier, J.; Bezzant, T.; Fletcher, T. H. Improved Method for the Determination of Kinetic Parameters from Non-isothermal Thermogravimetric Analysis (TGA) Data. *Energy Fuels* **2010**, *24* (5), 2841–2847.

Table 4. First-Order and DAEM Parameters Regressed for Oil Shale Samples

sample		first-order		DAEM	
		1 bar	40 bar	1 bar	40 bar
A	A (1/s)	6.99×10^{12}	1.29×10^{13}	2.67×10^{13}	6.33×10^{13}
	Ea (kJ/mol)	210.0	211.1	220.0	222.2
	σ (kJ)	~	~	2.7	1.7
B	A (1/s)	8.21×10^{12}	2.23×10^{13}	2.10×10^{13}	1.87×10^{14}
	Ea (kJ/mol)	210.0	212.4	213.4	225.6
	σ (kJ)	~	~	1.7	3.3
C	A (1/s)	5.04×10^{12}	7.36×10^{12}	2.69×10^{13}	1.35×10^{13}
	Ea (kJ/mol)	208.8	212.4	218.6	216.0
	σ (kJ)	~	~	2.6	2.4
1	A (1/s)	2.74×10^{10}	2.89×10^{10}	2.35×10^{12}	2.53×10^{12}
	Ea (kJ/mol)	175.9	174.8	202.5	201.8
	σ (J)	~	~	3.2	3.8
2	A (1/s)	1.79×10^{10}	3.04×10^{10}	2.01×10^{12}	2.85×10^{12}
	Ea (kJ/mol)	173.8	175.6	202.4	203.0
	σ (kJ)	~	~	3.8	4.4
3	A (1/s)	2.91×10^{10}	2.72×10^{10}	6.73×10^{12}	1.94×10^{12}
	Ea (kJ/mol)	177.0	176.9	208.8	202.1
	σ (kJ)	~	~	1.9	2.6

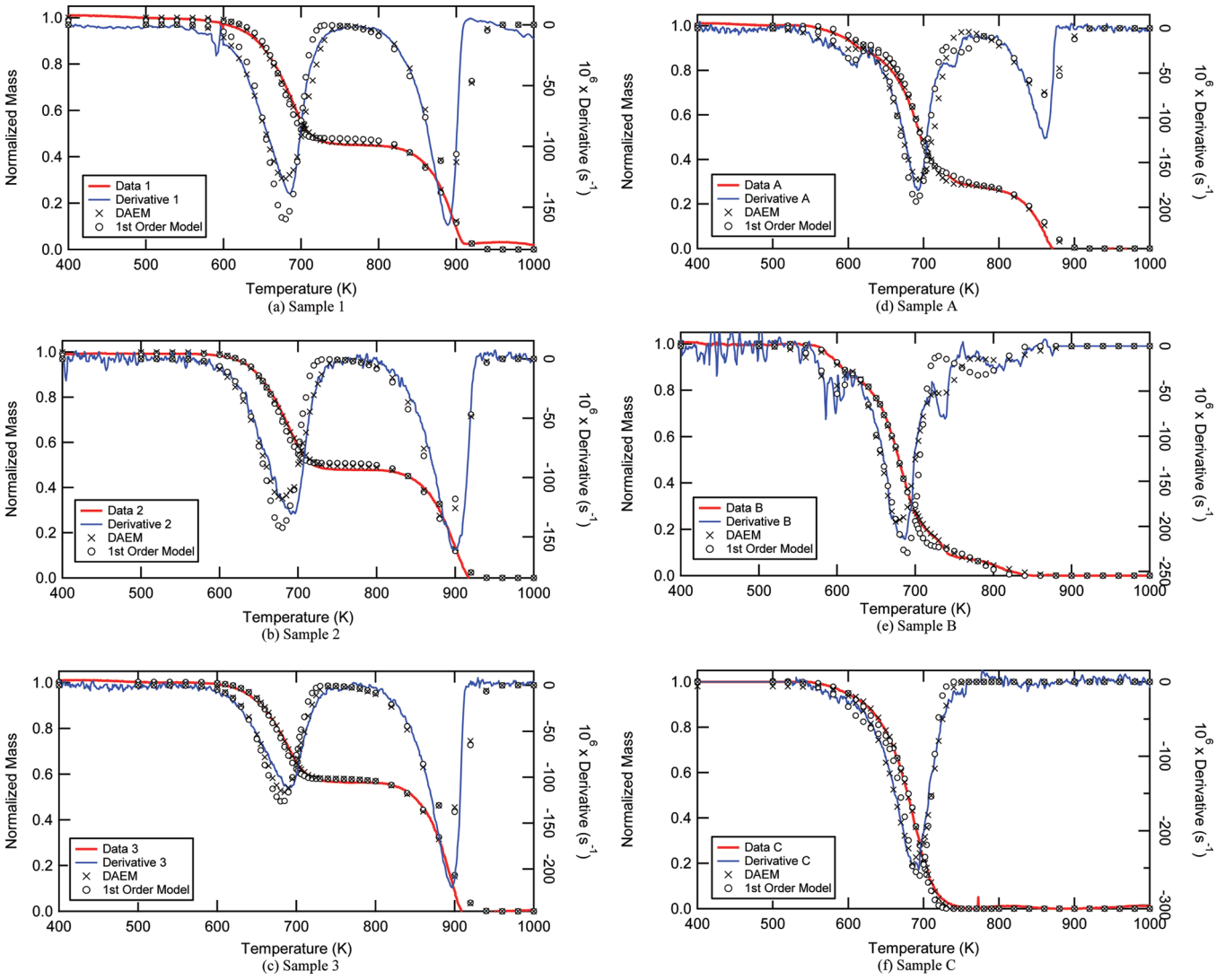

Figure 6. Comparison of model predictions and experimental data of both mass vs temperature (LHS) and derivative vs temperature (RHS) of each sample at 1 K/min, 1 bar conditions with model values being represented as a reduced number of points for clarity.

parentheses. For example, given the first-order model with an alpha of 0.5 the portion in the parentheses has a value of 3.57 for an n of 6 but falls to 1.23 for an n of 30 and approaches a value of 1.0 for an n of infinity. The other method of decreasing the critical value is to decrease the error associated with the optimal parameters (i.e., collect better data). Better

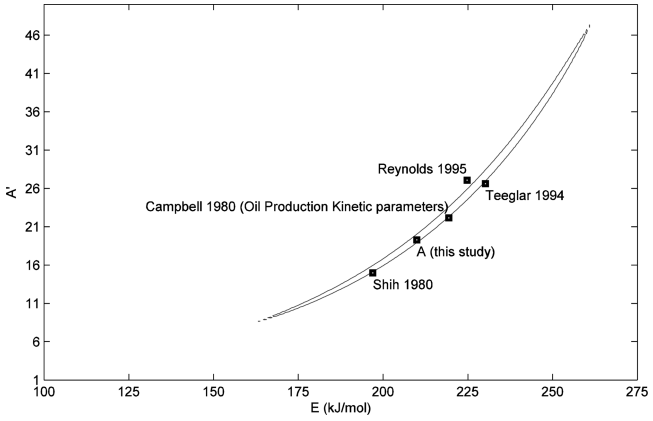

Figure 7. Statistical confidence region for Sample A with values from other researchers.

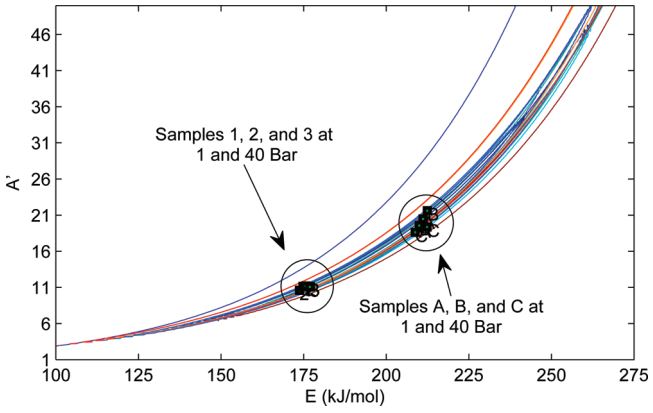

Figure 8. Confidence regions determined for the first-order model for 1 bar vs 40 bar with optimal points indicated.

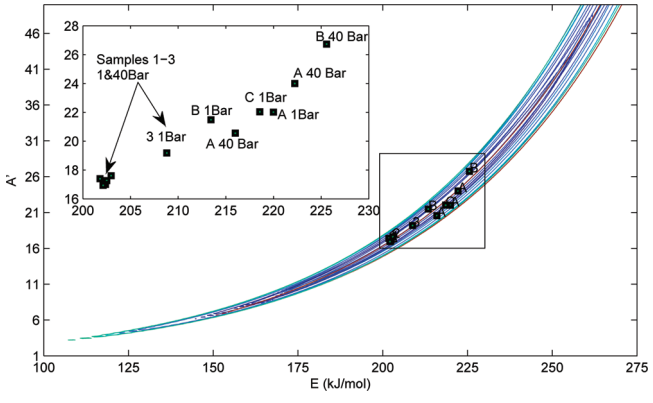

Figure 9. Confidence regions determined for the DAEM for 1 bar vs 40 bar with optimal points indicated and an insert for clarity to show the optimal points.

data would either be associated with lower noise and lower measurement errors or in the case of nonisothermal kinetic data it would be to have a wider spread in the heating rates. Unfortunately higher heating rates often are obscured by other effects such as mass transfer and hence there is an upper limit. Unfortunately lower heating rates become time-consuming and costly. The heating rates for this study were selected (as mentioned above) to span the widest range that would ensure no mass or heat transfer effects at the higher heating rates and to be performed in a reasonable time for the experimental

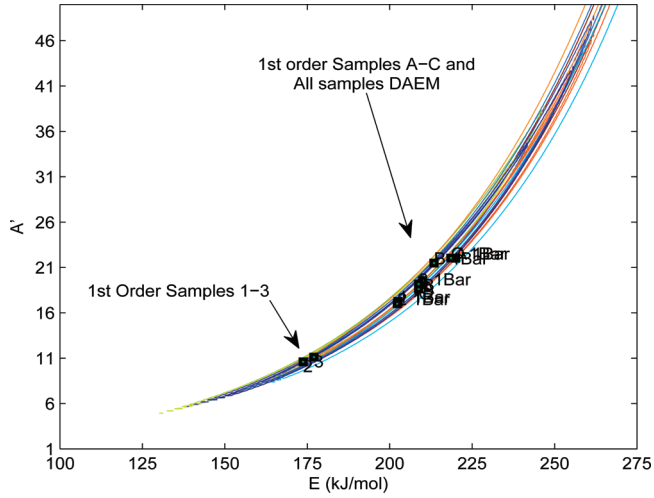

Figure 10. Confidence regions determined for the first-order model vs the DAEM at 1 bar with optimal points indicated. Note visually the overlap in the confidence regions.

setup at the lower heating rates. The resulting ideal parameters and confidence regions are seen here in Figures 7−10. For ease of visualization, a normalized value A' is used in these plots, defined as:

$$A'^{10} = A, \text{ or} \tag{6}$$

$$A' = 10^{(\log A)/10} \tag{7}$$

Figure 7 shows the confidence region for the Sample *A* (a GROS), the optimal first-order model parameters determined in this study, and several reported Green River Oil Shale parameters for the same model. The parameters all lie within or very close to the statistical confidence region and would each predict fairly well the pyrolysis and generation of oil shale at heating rates on the order of degrees per minute.

Figure 8 shows the comparison among the six samples at the two pressure levels for the first-order model. Note how the 40 bar data has much larger confidence regions. This is a result of the much larger noise in the 40 bar data. Despite the noise the ideal parameters for the different cases lie within each other's confidence regions indicating that the difference in the parameters is not statistically significant. This conclusion comes despite the numerical differences between Samples 1−3 and Samples A−C. There is a marked decrease in the magnitude of the kinetic parameters for Samples 1−3 and application of the parameters from Samples A−C to Samples 1−3 visually shows a poorer fit. The fact that they lie within each other's confidence regions could change if additional experiments allowed for smaller confidence regions, as explained above.

Note how the pressure may have a slight but not significant effect for the DAEM model and really no effect for the first-order model. This means at pressures expected at geological conditions or in many industrial situations the kinetic parameters determined at atmospheric conditions are sufficient. The stage of demineralization also does not appear to have a statistically significant effect, as indicated in Figures 8 and 9. This means that demineralization is not necessary for determination of kinetic parameters and that the oil product is not interacting with the minerals. Although the mass change above 800 K was fit with this procedure, the first-order or DAEM models did not seem to give adequate fits, and the results are not reported here.

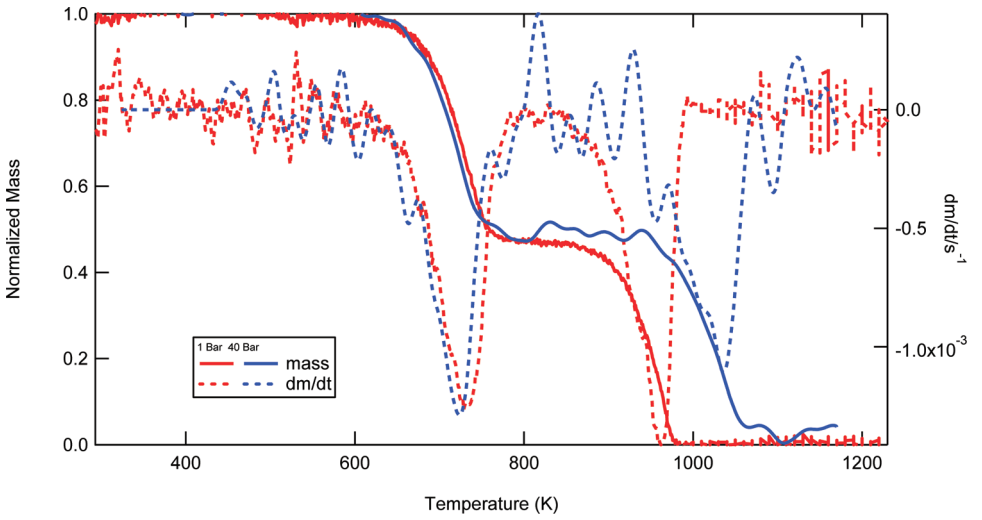

Figure 11. Comparison of mass and derivative traces for sample 1 at 1 bar and 40 bar. Note the similarities in both temperature and shape.

The pressure effect is negligible for the organic reaction. Figure 11 shows the TGA trace for same sample at the two different pressures. The slight difference in the two curves is really within the noise range for the 40 bar data and is not significant.

The DAEM model becomes a first-order model as the distribution approaches zero. The DAEM model is statistically significant in most of the cases considered in this work, but the overlap in the parameter confidence regions would indicate that it is only a small improvement over the first-order model. The result that a first-order model fits the data is similar to a result determined by Campbell and co-workers who examined a Colorado oil shale from Green River Formation.[6] It should be noted that the samples obtained from the surface showed a lower magnitude for the kinetic parameters (approximately 35 kJ/mol for the first-order model) than those from the core sample. The surface samples also showed a different TGA profile with only two distinct reactions instead of four. This reemphasizes that kinetic parameters can differ with sample composition. Further analysis could reveal the differences in the organic matter of the two samples despite both originating from the Green River formation. Despite the differences both show very similar confidence regions and that gives assurance that kinetic parameters obtained from a small sample can be used to adequately represent the larger formation.

The kinetics obtained from the three size-graded samples agreed well. The range for the first order on the kinetic parameters was 3.2 kJ/mol for the activation energy, with only a 38% variation in A at atmospheric and about a 10% variation in A at 40 bar pressure. The DAEM model showed very little distribution with σ on the order of 1.9−4.4 kJ. The improvement for the DAEM over the first order was statistically significant in each size-graded case but visually only showed minor differences. Because the kinetic parameters did not change much for the size-graded samples, it is assumed that mass transfer resistances at these heating rates were small.

The kinetics obtained from the successively demineralized samples also agreed well. The activation energy spanned 3.6 kJ. This range is within the error since the pre-exponential factor compensated. The improvement by using the DAEM for the demineralized series was much smaller and not statistically significant for Sample A at 1 bar and Sample B and C at 40 bar. The F value determined according to eq 4 was only barely above the critical F value for the cases where the F-test showed that the DAEM was statistically better for Samples A−C.

Conclusion

Crushed samples of Green Rive Oil Shale were pyrolyzed at heating rates from 1 to 10 K/min at pressures of 1 and 40 bar and temperatures up to 1000 °C. Two mass release peaks were observed corresponding to kerogen pyrolysis and carbonate decomposition for the size-graded sample. The demineralized sample came from a different location in the Green River formation and showed four peaks for sample A. Pyrolysis of samples from subsequent stages of demineralization showed three peaks for B and one peak (with a small shoulder) for C. The transient pyrolysis data were fit with a first-order model and a progressive Distributed Activation Energy Model (DAEM). An F-test was used to determine confidence regions and compare the kinetic parameters among the oil shale and demineralized samples, between the two pressure levels, and between the models.

The activation energies determined ranged from 173 to 226 kJ/mol, with most values around 200−220 kJ/mol. The kinetic coefficients determined for oil shale and the demineralized samples were statistically the same. Only small differences in kinetic coefficients were seen in the size-graded samples, indicating negligible mass transfer resistances at the heating rates used in these experiments. The difference in the kinetic coefficients for the pyrolysis at 40 bar was small (~3 kJ/mol) and not statistically significant. The first-order and DAEM models were also shown to be statistically different, but a visual inspection reveals that both models performed well. The largest effect was between the samples based on their parent sample. Those samples obtained from nearer the surface showed a lower set of kinetic parameters than those obtained from a core sample but the kinetic parameters were within the confidence region for the other samples so there is no statistically significant difference between the two.

Acknowledgment. We thank Dr. Ron Pugmire for the samples; James Orgill, Carl Isackson, Jeff Fletcher, Trent Bezzant, and Devon Rappleye for assisting in the data collection; and Chevron for funding the research.